The International Journal of Advanced Manufacturing Technology (2025) 136:413–431
https://doi.org/10.1007/s00170-024-14790-3

ORIGINAL ARTICLE

Performance evaluation of CrAlNAg-coated inserts with varying Ag content during roughing and finishing operations in face milling

Sumit Singh Rajput[1] · Chandramani Upadhyay[1] · Soumya Gangopadhyay[1] · Filipe Fernandes[2,3]

Received: 14 June 2024 / Accepted: 4 November 2024 / Published online: 22 November 2024

Abstract

The performance of a novel hard solid lubricant coating, CrAlNAg, in the face milling operation of AISI 1045 medium carbon steel under the modes of roughing and finishing was investigated. Dry machining was carried out using CrAlN coated inserts with varying silver (Ag) contents ranging from 0 to 16 at.%. The objective was to evaluate the performance of the developed coatings under different machining conditions, which could potentially result in (a) a high material removal rate (rough machining) and (b) high surface finish and dimensional accuracy (finish machining). An in-depth analysis of the cutting forces in face milling was performed to assess the impact of the coatings under these machining conditions. During machining, the force components in the *X*, *Y*, and *Z* directions were measured using a cutting force dynamometer attached to the workpiece. The components of these forces concerning the tool edge were calculated using geometrical characteristics and mathematical formulations, enabling the identification of the true cutting forces and the most sensitive force components relative to the cutting parameters. Apart from cutting forces, chip temperature, tool wear, surface roughness, and chip characteristics were evaluated for different coating compositions under both machining conditions. Owing to superior coating-substrate adhesion and tribological characteristics, the CrAlNAg9 coating with around 8.6 at.% of Ag was found to significantly reduce dominant forces and chip temperature under both machining conditions. Furthermore, the same coating exhibited remarkable resistance to flank wear compared to other compositions of CrAlNAg coatings.

Keywords Face milling · Roughing and finishing · CrAlNAg coatings · Cutting force · Chip temperature

Abbreviations

X, Y, Z	Coordinates of the reference system
F_x	Total force in X direction
F_y	Total force in Y direction
F_z	Total force in Z direction
F_{xy}	Resultant cutting force in XY plan with reference to workpiece
R	Resultant cutting force in XY plan with reference to tool
F	Friction force
N	Force normal to friction force
F_f	Feed force
F_n	Force normal to feed force
F_t	Tangential cutting force
F_r	Radial cutting force
F_p	Thrust force
F_{xy}	Resultant force
V_c	Cutting speed
f_r	Table feed rate
f_z	Feed/tooth
a_e	Radial depth of cut
a_p	Axial depth of cut
ϕ	Angle of rotation during entry
L	Cutting length
L_c	Critical load
COF	Coefficient of friction
VB	Flank wear
μ	Coefficient of friction
h_{ch}	Maximum chip thickness
P_c	Saw-tooth distance
at.%	Atomic percentage

✉ Soumya Gangopadhyay
soumya@iitbhilai.ac.in

[1] Department of Mechanical Engineering, Indian Institute of Technology Bhilai, Durg 491002, Chhattisgarh, India

[2] CIDEM, ISEP - Polytechnic of Porto, Rua Dr. António Bernardino de Almeida, 4249-015 Porto, Portugal

[3] University of Coimbra, CEMMPRE, ARISE, Department of Mechanical Engineering, Rua Luís Reis Santos, 3030-788 Coimbra, Portugal

1 Introduction

Milling is a machining process that removes material from a workpiece, producing various surfaces, such as flat, curved, and complex shapes [1]. It is widely used in manufacturing to create precision parts and components in various industries. Traditionally, cemented carbide tools have been the tools of choice for milling operations owing to their high toughness [2, 3]. However, the insufficient wear resistance of cemented carbide tools operating at high speeds has limited their applications. To overcome this, advanced tool materials such as cubic boron nitride (CBN) and ceramic tools have been employed, especially for high-speed milling [4, 5]. However, these cutting tools are very expensive and normally not suggested for low-speed machining applications.

In industry, roughing operations are performed to remove excess material from the workpieces quickly by incorporating high feed and depth of cut, imparting the subsequent machining operations (finishing) faster and more efficiently, whereas finishing operations were carried out at high speed with low feed and depth of cut to meet the product requirements such as flatness, tolerances, and surface finishes. Both operations stand different in terms of machining parameters and tool wear phenomena and mostly require specific tools [6, 7]. To address these challenges altogether, the development of hard coatings for carbide tools has emerged as a more cost-effective and versatile solution [7–10]. Hard coatings not only enhance the wear resistance of carbide tools but also expand the range of operating conditions, making them suitable for both high-speed and low-speed operating conditions.

The current manufacturing industry, focusing on cutting costs and promoting eco-friendly practices, has led to a significant increase in the use of dry machining methods. Dry machining minimizes or eliminates the use of cutting fluids, reducing both operational costs and environmental impacts [11]. This can be achieved by incorporating hard coatings that deliver superior hardness and tribological properties to tools. The machining industry already has various hard coatings that can be used, owing to their specific advantages. For example, TiNand TiAlN coatings improve wear resistance and hardness, whereas AlTiN coatings also improve oxidation resistance [12–17]. In a study by Rodríguez-Barrero et al. [18], TiAlSiN, AlTiSiN, and μAlTiN were found to be suitable in the drilling of medium carbon steel 42-CrMo-4. Improved performance of the coatings was achieved after the removal of surface droplets by the drag grinding process. When some elements like Si and V were added to TiAlN, hardness and wear resistance properties were improved by Si addition, while low friction properties were achieved at a high temperature due to the inclusion of V. These TiAlSiVN coatings demonstrated improvement in anti-friction properties with reference to TiSiN coating during the turning of Ti6Al4V, particularly in terms of reduction in material adhesion. The same TiAlSiVN coatings with varying contents of V resulted in a reduction in cutting forces in the range of 27 to 34% with reference to uncoated tool [19–22]. Some other coating families, such as DLC and WC/C combined, improved the wear resistance and anti-friction properties of the tools [23]. However, the current study focused on chromium aluminum nitride (CrAlN) coating because of its exceptional oxidation resistance, thermal stability, and hardness. These coatings formed a protective $(Al,Cr)_2O_3$ oxide layer at an early stage of the oxidation process. This layer effectively prevents further oxygen penetration and restricts the outward diffusion of metallic ions [24–26]. As a result, it enhances the durability and stability of the coating at high temperatures. Researchers have observed significant improvements in tool life and machining performance while using CrAlN coatings in both roughing (low speed with high feed and depth of cut) [27, 28] and finishing (high speed with low feed and depth of cut) [29, 30] operations. It was also reported in the literature that the mechanical properties of CrAlN can be optimized by carefully adjusting the aluminum content, making these coatings particularly suitable for cutting tool applications [31].

CrAlN coatings doped with silver (Ag) have demonstrated considerable potential. Silver is a highly promising candidate because of its outstanding lubricating properties, which are largely due to its high ductility at elevated temperatures [32–34]. This ductility allows silver to undergo plastic deformation, facilitating smooth shear between sliding surfaces and thereby providing effective lubrication [32–34]. Additionally, the thermochemical stability of silver, particularly its resistance to oxidation at high temperatures [35], ensures that it maintains its lubricating capabilities across a wide range of temperatures. Researchers have shown that silver can significantly reduce friction at both room and high temperatures [32, 36–38]. Therefore, doping Ag into the CrAlN matrix is anticipated to diminish friction and wear during machining operations, thus enhancing tool performance in terms of wear resistance and surface finishing.

An in-depth study of Ag-doped CrAlN coatings under both roughing and finishing machining conditions has not yet been reported. The current research work addresses this gap by focusing on the development and performance evaluation of CrAlNAg-coated inserts with varying silver content during both machining operations, which are extensively utilized in the industry. Specifically, the study aims to compare the coated tools' performance in terms of cutting force, chip temperature, surface finishing, and chip formation. Through this comparative analysis, the optimal silver content in the

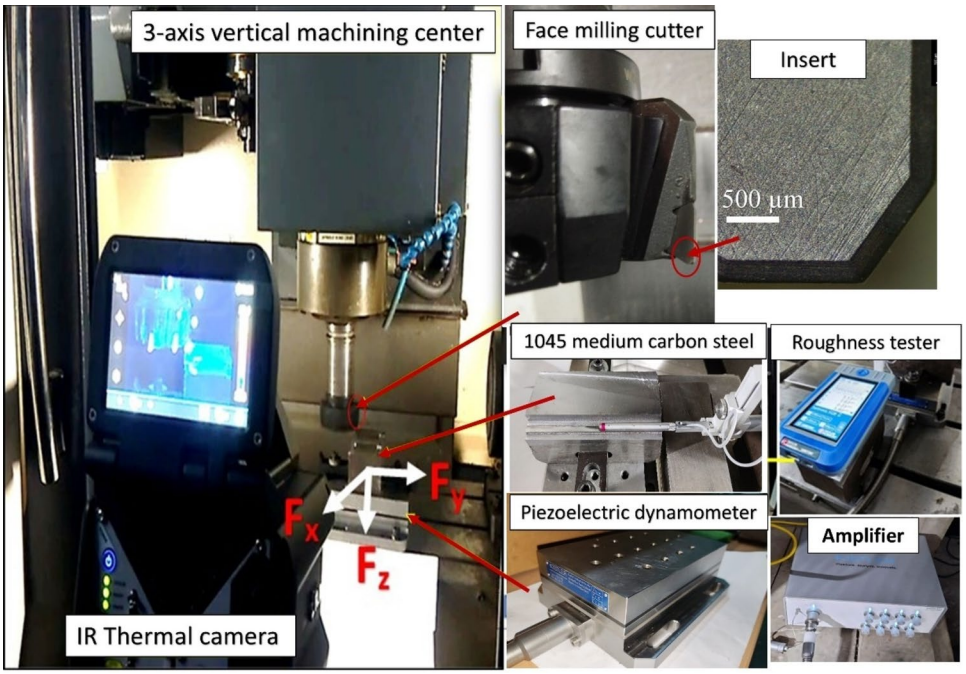

Fig. 1 Experimental setup during face milling

Table 1 Tool inserts and holder specifications

Inserts	Tool holder details
Designation TPAN1603PPN THM T: Inserts shape (triangular) P: Clearance angle (11°) A: Tolerance class N: Fixing (no hole) 16: Cutting edge length (16.453 mm) 03: Thickness (3.18 mm) P: Corner configuration (11°) P: Cutting edge condition N: Direction of cutting (neutral) Grain size: 1.2–2 µm	Designation M40-TP16 Cutter diameter: 85 Rake angle: 0° Maximum depth of cut: 13 Total inserts accommodation: 5

CrAlN coating that maximizes the machining performance and extends tool life under dry machining conditions can be determined.

2 Materials and methods

2.1 Cutting tool preparation and testing

The cutting tools used in this experiment were tungsten carbide (WC) inserts (as shown in Fig. 1) of TPAN1603PPN designation, mounted on the milling cutter manufactured by WIDIA, for face milling operations. Further information regarding the tool inserts and the tool holder is provided in Table 1. All received tools underwent coating deposition after an initial preparation phase, which involved cleaning them in an ultrasonic bath with ethanol and acetone for 20 min each. The tools were then grouped into specific batches of coating deposition. The deposition process was carried out using a multi-target HiPIMS coating system developed by Teer Coatings Ltd., UK. The initial steps involved deploying Cr, Al, and Ag targets, along with the substrates (tool inserts), at their designated positions in the coating chamber. An ion-etch cleaning process was then performed at a base pressure of 4×10^{-6} Pa with a substrate bias of −600 V, using Ar^+ as an etching agent. Following this, the

Table 2 Coating designation, chemical composition and hardness of the CrAlNAg coatings

Sample	Cr (at.%)	Al (at.%)	N (at.%)	Ag (at.%)	O (at.%)	Hardness (GPa)
CrAlN	37 ± 0.4	10.9 ± 0.2	50.0 ± 0.4	0	2.1 ± 0.08	18.0 ± 3.2
CrAlNAg2	36 ± 0.8	10.4 ± 0.2	48.8 ± 0.23	2.4 ± 0.1	1.9 ± 0.09	17.0 ± 2.6
CrAlNAg9	34 ± 0.65	9.9 ± 0.1	45.7 ± 0.18	8.6 ± 0.2	1.7 ± 0.09	23.0 ± 3.3
CrAlNAg12	32 ± 0.5	9.3 ± 0.2	44.1 ± 0.2	11.8 ± 0.22	2.0 ± 0.06	19.9 ± 3.3
CrAlNAg16	31 ± 0.30	9.1 ± 0.08	42.1 ± 0.25	15.8 ± 0.32	1.8 ± 0.08	14.4 ± 3.1

Table 3 Chemical composition of the workpiece

Element	Fe	C	Si	Mn	Cu, Cr	Ni	P, S
Component (wt.%)	99	0.42–0.50	0.17–0.37	0.5–0.8	≤0.25	≤0.30	0.035

Table 4 Some relevant properties of AISI 1045 medium carbon steel

Poisson's ratio	0.3
Tensile strength (MPa)	570–700
Brinell hardness	170–210
Elastic modulus (GPa)	200
Density (kg/m^3)	7800–7850
Thermal conductivity (W/(mK))	38

final coating deposition was achieved by adjusting the power supplied to the Ag targets, resulting in coated tool inserts with varying Ag content. All the deposition parameters were set by considering the authors' previous research work [24] which may be referred to for detailed information. The coating thickness was determined using the fractography technique followed by examination using field emission scanning electron microscopy (FESEM Gemini500; Zeiss, Germany). Furthermore, the cohesion strength and adhesion of reference CrAlN and CrAlNAg-coated inserts were evaluated using a TR-101 scratch tester manufactured by Ducom, India. A scratch velocity of 0.2 mm/s was applied over a stroke length of 10 mm, with a loading rate varying to 1.2 N/s for normal loads ranging from 20 to 80 N. An optical microscope (Leica, Model: S9i) was utilized to capture images of the scratch tracks. The critical load values were determined from these images by identifying the points at which failure was initiated. The chemical composition and hardness of the developed coatings are presented in Table 2.

2.2 Workpiece material

Machining was carried out on AISI 1045 medium carbon steel, a widely used material for components such as crankshafts, gears, bolts, and connecting rods [34, 39]. This high-quality carbon structural steel has low hardness and is easy to cut. All workpiece surfaces underwent milling treatment before final machining to remove the original surface oxides and hard spots. Also, the workpiece dimensions were reduced to 120 mm × 360 mm × 360 mm so that it could be fixed on the top of the dynamometer. Some relevant information related to the workpiece, such as chemical composition and mechanical properties, are listed in Tables 3 and 4, respectively.

2.3 Experimental setup and procedures

2.3.1 Machining conditions

All the milling tests were carried out on a 3-axis Computer Numeric Control (CNC) vertical machining center (AMS 540V) with Fanuc controller developed by Ace Micromatic, India, as presented in Fig. 1. The machine has a maximum power capacity of 5.5 kW and a maximum rotation speed of 6000 rpm. The machining parameters presented in Table 5 were selected to reflect two different types of machining, commonly known as roughing and finishing. The milling operation was performed using a face milling cutter capable of accommodating five tools simultaneously. However, only one milling insert was used at a time to critically evaluate the cutting force, tool wear, and surface finishing during machining. During milling, care was taken to ensure that the rotating cutter smoothly engaged and disengaged from the workpiece to prevent sudden forces that might affect the tool. The tests were performed with all the developed coatings and were repeated three times to ensure the accuracy of the output results. All the milling operations were tested in dry conditions to critically evaluate the machining performance of the coatings without the interference of lubricants. The details of the roughing and finishing modes of milling operations are provided in Table 5.

2.3.2 Cutting forces and temperature measurements

The cutting force measurement setup installed alongside the milling center is presented in Fig. 1. This setup features the Kistler 9257B three-component force dynamometer, which includes an A/D data acquisition board for converting force signals into electrical signals, and a Kistler 5001A charge amplifier for signal amplification. The sampling frequency was configured to 1000 Hz for this test. Real-time forces in the F_x, F_y, and F_z directions were recorded using the Dyno Ware software. An infrared (IR) camera (X6540sc; FLIR, US) was used to measure the maximum temperature of the generated chips, which was capable of accurately recording temperatures from 350 to 1200 °C. The emissivity of the workpiece, determined through several calibration experiments, was assumed to be approximately 0.8 during the testing.

All inserts with different coating compositions were deposited using the same deposition procedure. During milling also, it was ensured that all tests were performed under the specified parameters. This guarantees that any changes in cutting forces

Table 5 Experimental parameters for different machining conditions

Machining condition	V_c (m/min)	f_r (mm/min)	f_f (mm/tooth)	a_p (mm)	a_e (mm)	L (mm)	Total pass
Roughing	75	300	1.0676	1	5	120	6
Finishing	250	50	0.0534	0.4	5	120	6

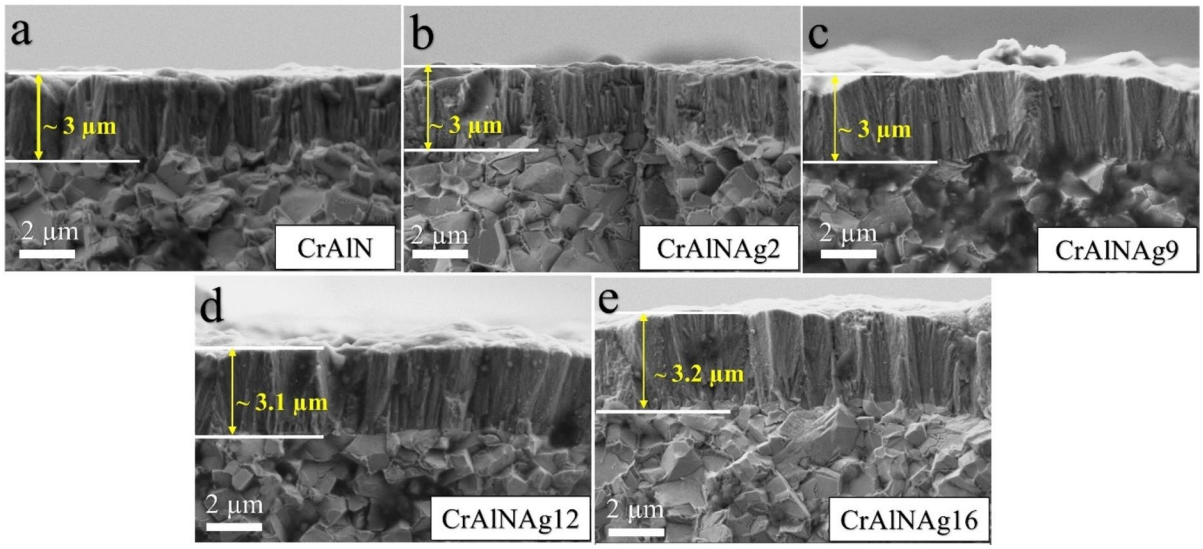

Fig. 2 Fractography of CrAlNAg coatings with varying contents of Ag deposited over milling inserts

or tool wear behavior in both testing conditions are induced only by the coating properties. To ensure reliable data collection, a new cutting tool was employed for each experiment. In addition, all measurements were performed three times to enhance accuracy, and the arithmetic mean values of the cutting forces were subsequently calculated.

2.3.3 Surface roughness, chip thickness, and tool wear

Surface roughness tests were conducted on the machined surface using a Surtronic S-100 surface roughness tester manufactured by Taylor Hobson, UK. During the measurement, sampling length and cut-off length were set to 0.8 mm and 4 mm, respectively, whereas the arithmetic mean of surface roughness (R_a) was used to represent the surface roughness of the machined surface. Optical images of the machined chips were captured using a stereo-zoom microscope. During roughing mode of machining, the chips' maximum cross-section thickness was measured using a C/N 342–251-30 µm made by Mitutoyo, Japan, with having the least count of 0.001 cm. Further, to ensure statistical reliability, each measurement was repeated at least five times to accurately assess surface roughness and chip thickness. Assessment of tool wear phenomena such as flank wear, material adhesion, and coating removal were examined using SEM, whereas elemental mapping of the coated inserts was inspected using energy dispersive spectroscopy (EDS).

3 Results and discussion

3.1 Characterization of the coatings

CrAlNAg coatings with different Ag content were deposited using HiPIMS technology. The fractography method was applied to examine the thickness of the deposited coatings and is presented in Fig. 2. The coating exhibits a nearly uniform thickness, although it is slightly thicker in CrAlN coatings with higher Ag content, such as CrAlNAg12 and CrAlNAg16. The coating that has Ag up to 9 at.% shows dense columnar structure morphology that improved the hardness of the deposited coating [24]. However, it was observed that a higher amount of the soft phase causes a transformation from a dense to a more distinctive columnar structure. Increasing the Ag concentration in the coating during deposition increased the number of nucleation sites. Due to the high mobility of Ag, it tends to segregate and coalesce into larger particles. These particles exhibit poor affinity for other metallic compounds, leading to the formation of a porous and spontaneous morphology.

The adhesion property of various coating architectures was evaluated using scratch adhesion tests. Figure 3 illustrates the profiles of scratches for the reference CrAlN and coating with Ag variation. The scratch profiles illustrate the variation in traction force and coefficient of friction as

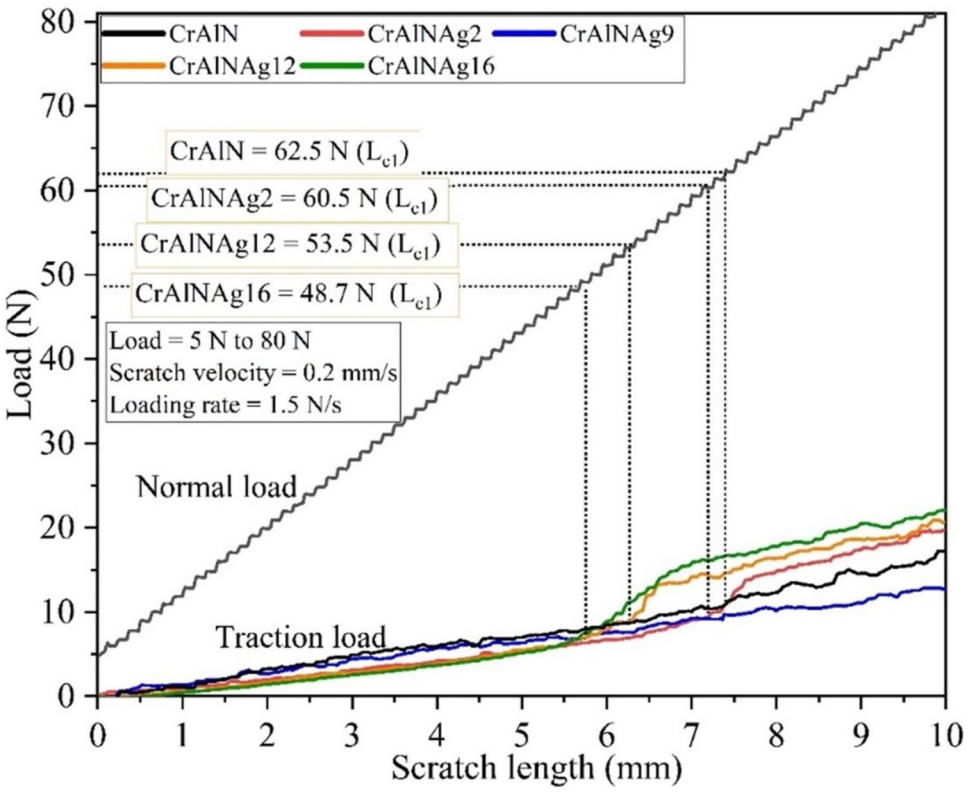

Fig. 3 Variation of load with scratch length during the scratch test of the coatings

the normal load increased at a constant rate, with a 200 µm diameter diamond indenter moving across the coated specimens. A sudden rise in the traction force or coefficient of friction in the scratch profile indicates the onset of coating delamination, and the corresponding normal load was termed the critical load (L_c). The results revealed that the CrAlNAg9 coating exhibited the best adhesion strength, showing no signs of failure during testing. This was followed by the reference CrAlN coating with a critical load measured at approximately 62.5 N and the Ag-doped CrAlNAg2 coating with a critical load of approximately 60.5 N. The improved adhesion in the CrAlNAg9 coating was attributed to the compactness and grain refinement resulting from the optimal addition of Ag, which enhances the adhesion of the coating to the substrate. Conversely, an excessive amount of the soft phase (high Ag content) weakens the coating's adhesion. Hence, the coating with the highest Ag content, CrAlNAg16, exhibited the weakest adhesion, with a critical load of approximately 48.7 N.

Figure 4 shows optical microscope images of the scratch tracks for reference CrAlN and CrAlNAg coatings with different silver contents, deposited on WC substrates. The images highlight the initial, mid, and end sections of the scratch tracks. The visual appearance indicated delamination of the CrAlNAg12 and CrAlNAg16 coatings around the mid-portion (between 5 and 6 mm of scratch length), as shown in the figure. In contrast, the CrAlNAg2 coatings showed failure at the end of the scratch. To confirm these observations, EDS analysis was performed on some coatings, such as CrAlNAg9 and CrAlNAg12, as depicted in Fig. 5. The analysis clearly showed that the CrAlNAg12 coating started delaminating at region 1 near the mid-portion, whereas the CrAlNAg9 coating remained almost intact till the end of the scratch (region 2). It is worth noting that the presence of nitrogen in the EDS analysis indicated the retention of the CrAlNAg9 coating till the end of the test.

3.2 Milling performance of the coatings in roughing and finishing operations

3.2.1 Cutting forces

An illustrative image showcasing coated milling inserts is displayed in Fig. 6 along with different cutting forces acting on the tool under roughing and finishing conditions. Additionally, the schematic representation in the same figure illustrates the position of the workpiece (AISI 1045 steel) along with the depth of the cuts during the roughing and finishing operations. The utilized milling insert

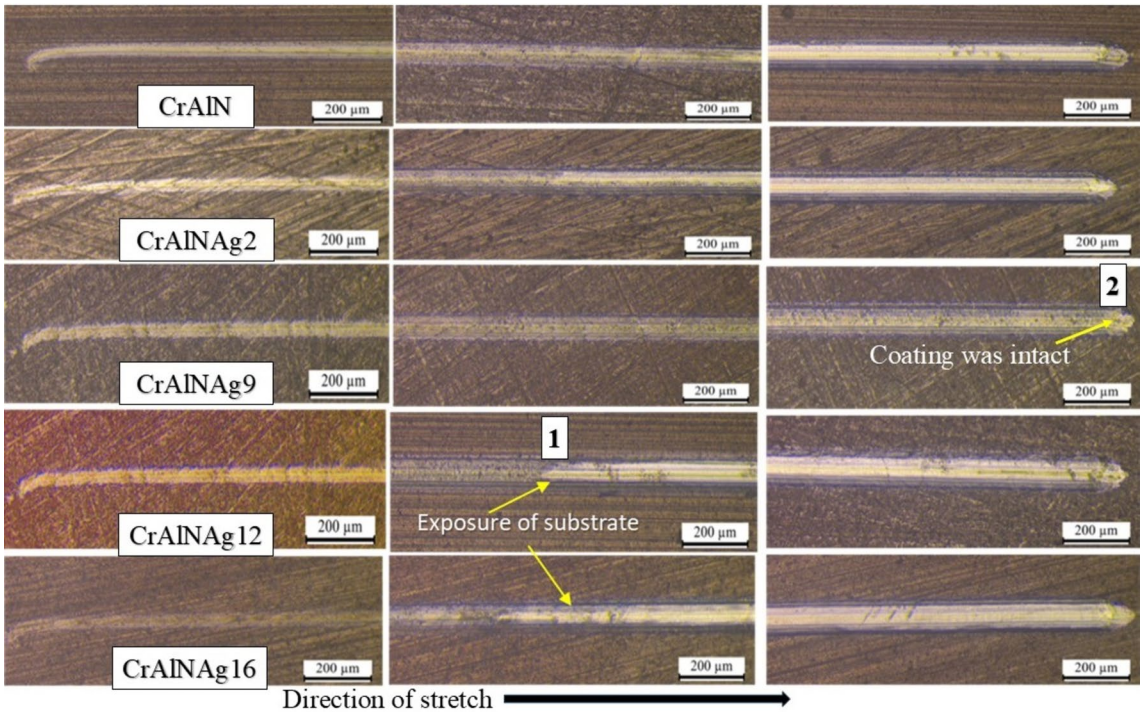

Fig. 4 Optical microscopic images of scratches performed on CrAlNAg coatings

features a wiper cutting edge, as indicated in the figure, aimed at enhancing the surface finish. The length of the wiper cutting edge, referred to as the parallel land (b_s), replaces the auxiliary cutting edge of conventional milling inserts. Figure 6 depicts both the main and auxiliary cutting edges of the milling inserts with wiper geometry. In roughing operations, which involve an axial depth of cut (a_P) of 1 mm, both the main and auxiliary cutting edges contribute to the cutting process. However, during finishing operations with an axial depth of cut (a_P) reduced to 0.4 mm, only the main cutting edge is engaged. This unique tool geometry significantly influences the distribution of cutting forces, as illustrated in Fig. 6.

The different cutting forces in the X, Y, and Z directions, that is, F_x (along the direction of table feed), F_y (perpendicular to the direction of table feed), and F_z (along the cutter axis) were directly measured by a dynamometer. Under roughing conditions, since the contribution of the auxiliary cutting edge was significant, the influence of F_x and F_y on the overall cutting force was greater. However, no participation of the auxiliary cutting edge was found under finishing conditions. In the absence of F_{x2} and F_{y2}

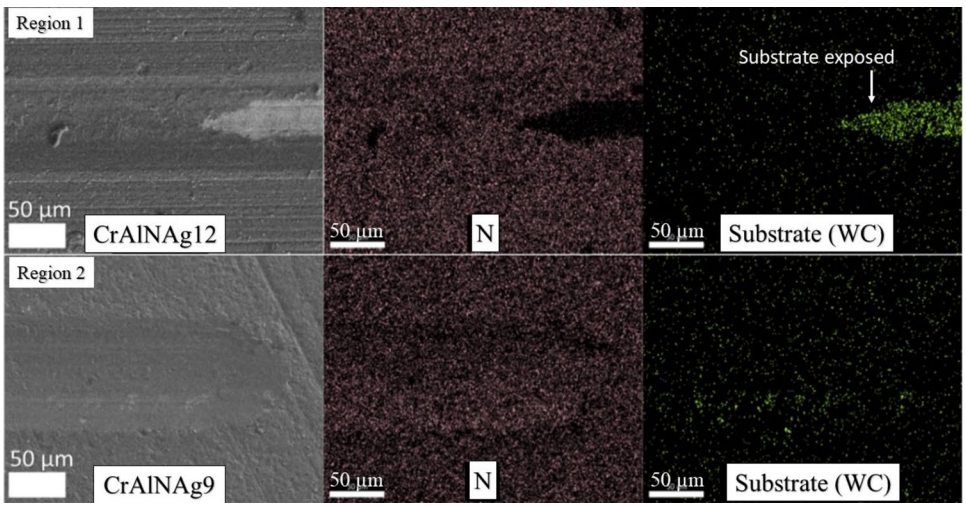

Fig. 5 Representative SEM images along with elemental mapping of region-1 of CrAlNAg12 and region-2 of CrAlNAg9 coatings as mentioned in Fig. 4

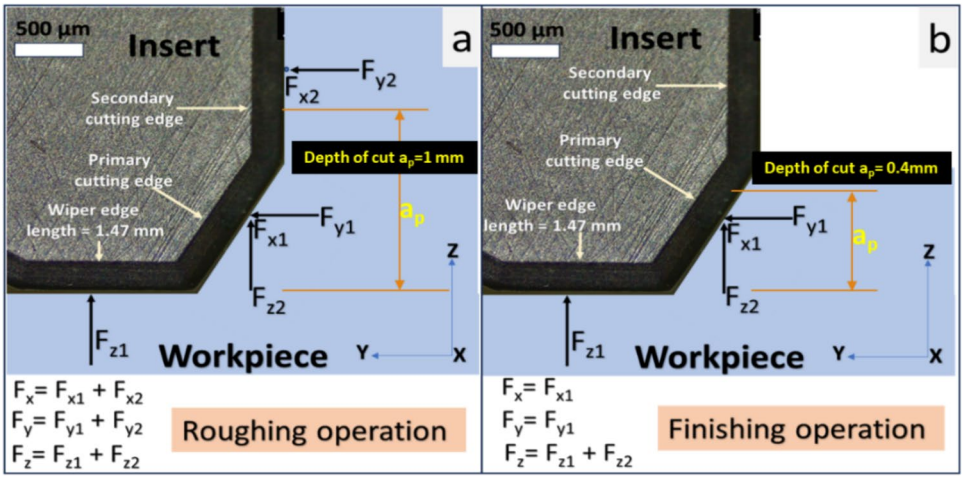

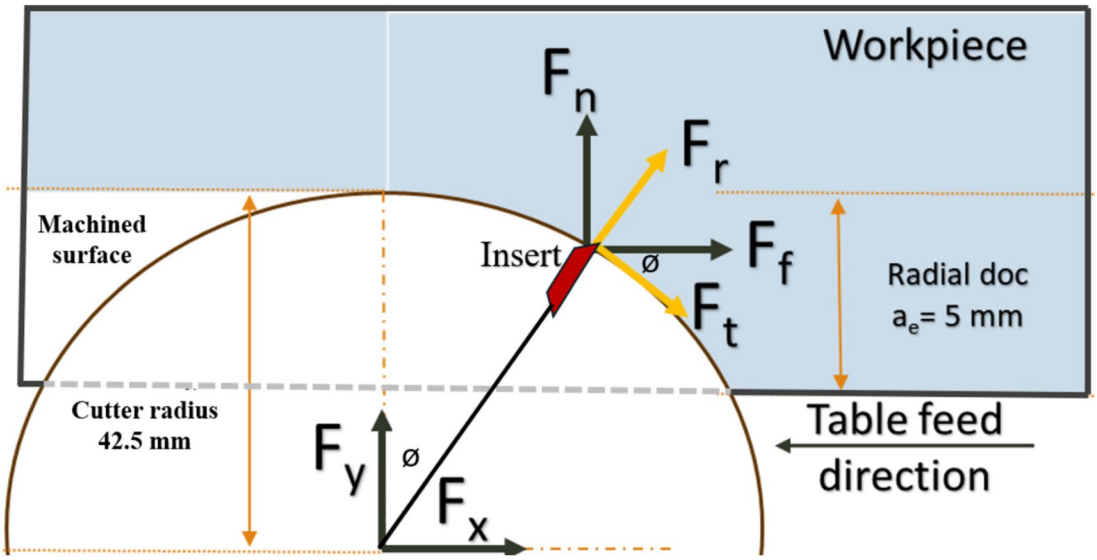

Fig. 6 Schematic representation of cutting forces acting on the workpiece under **a** roughing and **b** finishing conditions

Fig. 7 Schematic representation of cutting force components acting on the cutting edge during the face milling operation

(Fig. 6) under finishing conditions, F_z played a more dominant role in determining the overall cutting force. Additionally, the tool geometry of milling inserts with a wiper edge also influences the surface roughness, a topic that will be further discussed in a later section.

Figure 7 depicts a schematic representation of cutting forces concerning the cutting tool edges in face milling operations. These force components are typically defined in a different coordinate system in milling operations, denoted as F_t (tangential cutting force), F_r (radial force), and F_p (passive force). However, due to the dynamic nature of milling operations, there are discrepancies between the forces measured in these two coordinate systems [40, 41]. Under the current scheme of an experiment, the radial depth of cut was always smaller than the radius of the tool holder (42.5 mm), thus maintaining the up milling condition throughout. As a result, machining occurred solely during the forward half of each rotation, whereas no machining was carried out during the second half.

Representative signals of cutting forces of the first run during machining with reference to CrAlN coating are presented in Fig. 8. The highest force (F_x) was observed in the direction of the table feed motion, whereas the lowest force (F_z) was evident along the cutter axis. These observations were made under specific cutting parameters, where the radial depth was less than one-fourth of the cutter diameter. This cutting configuration involves the tool in the feed direction during cutting. This may be the possible reason for having a higher force (F_x) value in the table feed direction. However, for the finishing operation, it can be seen from the same figure that F_z became more dominant due to the reduced contribution of F_x and F_y in the absence of the

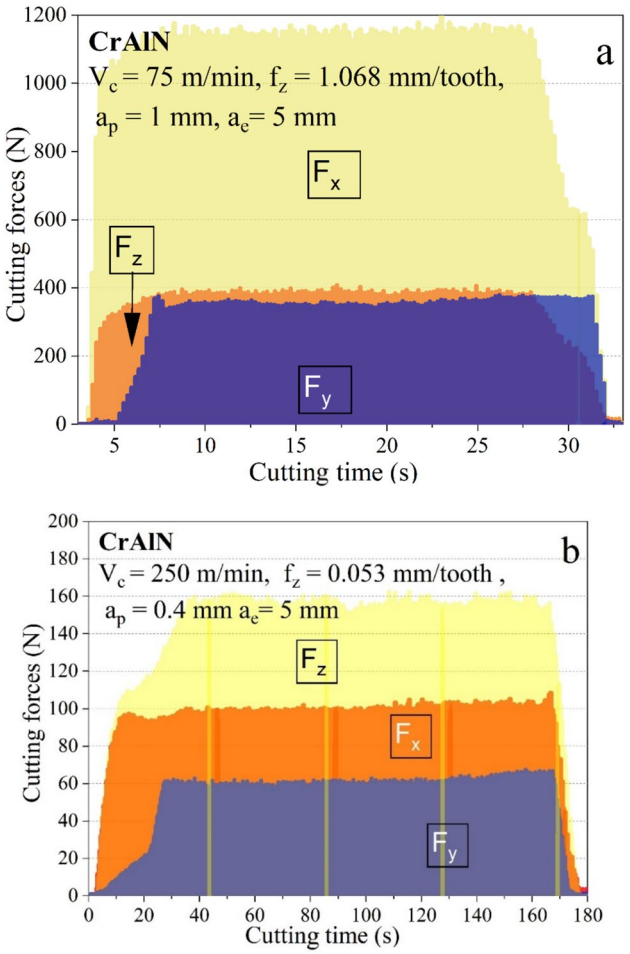

Fig. 8 Representative profiles of cutting forces (F_x, F_y, and F_z) under **a** roughing and **b** finishing conditions machined with reference CrAlN-coated milling insert

participation of the auxiliary cutting edge under the same conditions. Moreover, all the force components involved in the finishing condition were lower than those in the roughing mode of machining, attributed to the thermal softening that takes place at high cutting speed [42, 43]. This variation in force components affects the tool wear mechanism and chip formation, which will be discussed in a later section.

The force signals shown in Fig. 8 were further amplified to illustrate the discontinuous nature of contact in the milling operation. The same is depicted in Fig. 9 under roughing and finishing conditions. The frequency of the force signals is obviously higher in the case of the finishing operation due to the increased cutting speed compared to the roughing operation. Figure 9 further reveals that under roughing, the F_x signal gradually increases followed by a sharp fall, while the F_y signal exhibits the opposite pattern. It was due to the fact that at the point of entry, F_y is always maximum which gradually gets converted into F_x at the point of exit. Furthermore, due to lower cutting speed under roughing conditions, the tool engagement is slower than in finishing conditions. This phenomenon distinguishes the nature of curves for F_x and F_y under roughing and finishing operations. The nature of F_z signal followed a similar trend to that of F_x as also demonstrated by Li et al. [44].

Variations in cutting forces generated during face milling with coated tool inserts under both roughing and finishing conditions are presented in Fig. 10. In roughing conditions (Fig. 10a), CrAlNAg9-coated inserts performed better in reducing cutting forces, followed by the CrAlNAg16 coating. Specifically, the CrAlNAg9 coating reduced F_x by approximately 10% and F_y by around 4.5% compared to the reference CrAlN coating. The CrAlNAg16 coating achieved a reduction of 8% in F_x compared to the reference CrAlN coating. The results indicate that F_x played a major role in modifying friction at the chip-tool interface.

For finishing conditions also, CrAlNAg9 coating outperformed all the other coatings and reduced F_z by 15.5% compared to CrAlN coating. Other CrAlNAg coatings were not effective in reducing any of the force components during the experiments. The superior anti-friction properties of CrAlNAg9 coating may be responsible for the effective reduction in cutting forces. In contrast, the other Ag-doped coatings did not exhibit promising tribological behavior, either due to unfavorable oxidation or higher specific wear rates associated with higher Ag content. It should be noted that frictional drag at the chip-tool interface is more significant at lower cutting speeds, as reported by the other researchers [45, 46].

From Fig. 7, the tool-referenced force components can be derived by converting the dynamometer force components.

$$F_t = F_x \cdot \cos(\varphi) + F_y \cdot \sin(\varphi) \tag{1}$$

$$F_r = F_x \cdot \sin(\varphi) - F_y \cdot \cos(\varphi) \tag{2}$$

$$F_p = F_z \tag{3}$$

$$F_{xy} = \sqrt{F_x^2 + F_y^2}$$

From equation

$$F_t = F_x \cdot \cos(\varphi) + F_y \cdot \sin(\varphi)$$

$$= F_{xy} \cdot \left(\frac{F_x}{F_{xy}} \cdot \cos(\varphi) + \frac{F_y}{F_{xy}} \cdot \sin(\varphi) \right)$$

We know that

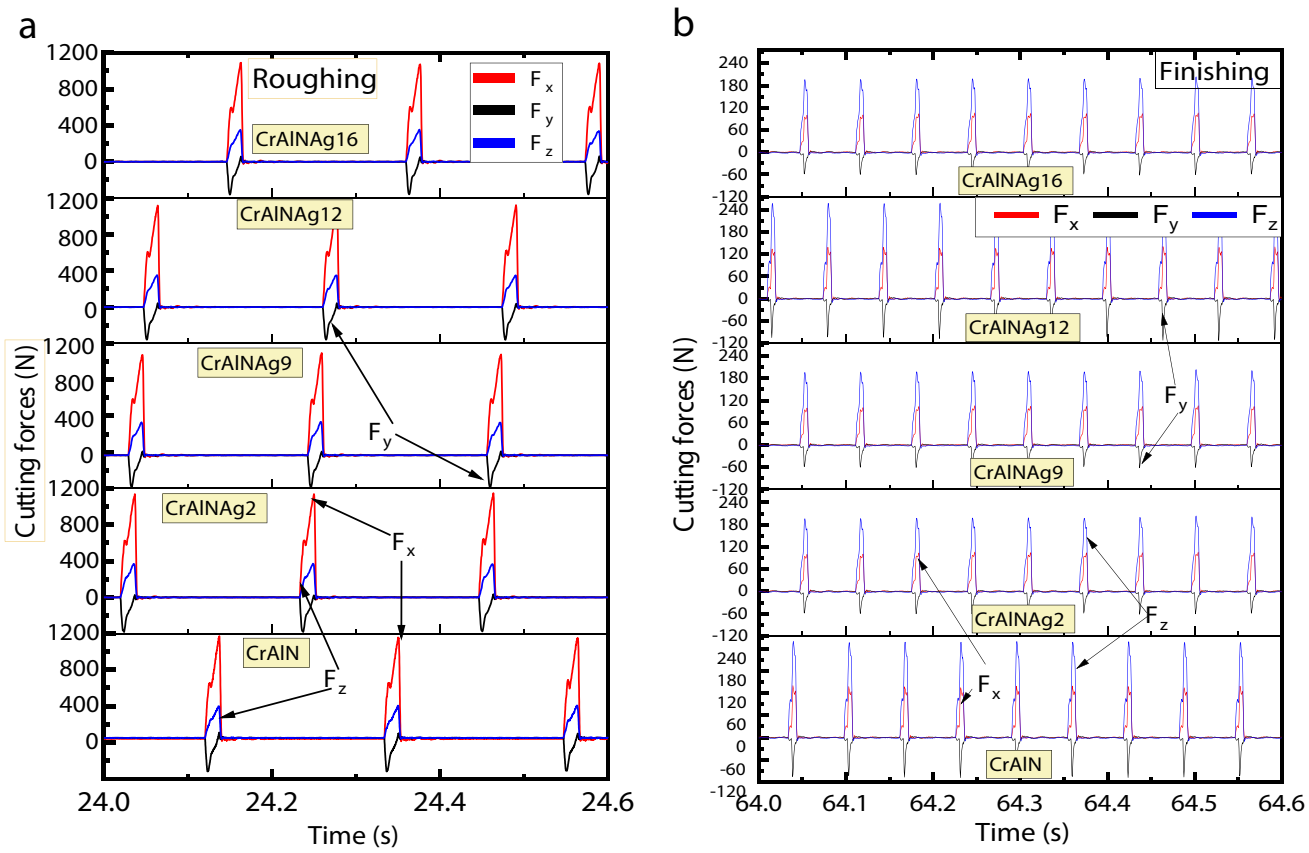

Fig. 9 Amplified cutting force signals during face milling using different coated tools while operating at **a** roughing and **b** finishing conditions

$$\sin\left(\arctan\left(\frac{F_x}{F_y}\right)\right) = \frac{F_x}{F_{xy}} \tag{4}$$

$$\cos\left(\arctan\left(\frac{F_x}{F_y}\right)\right) = \frac{F_y}{F_{xy}} \tag{5}$$

Incorporating values from Eq. (4), we obtain

$$\frac{F_r}{F_{xy}} = \sin\left(\arctan\left(\frac{F_x}{F_y}\right)\right)\cdot\cos(\varphi) + \cos\left(\arctan\left(\frac{F_x}{F_y}\right)\right)\cdot\sin(\varphi)$$

Using the angle addition formula for sine, we obtain

$$= \sin\left(\arctan\left(\frac{F_x}{F_y}\right) + \varphi\right)$$

Further resolving the equation,

$$= \sin\left(180^\circ - \arctan\left(F_x/F_y\right) - \varphi\right)$$

$$F_t = F_{xy}\sin\left(180^\circ - \arctan\left(F_x/F_y\right) - \varphi\right) \tag{6}$$

Similarly,

$$F_r = F_x\cdot\sin(\varphi) - F_y\cdot\cos(\varphi)$$

$$= F_{xy}\cdot\left(\frac{F_x}{F_{xy}}\cdot\sin(\varphi) - \frac{F_y}{F_{xy}}\cdot\cos(\varphi)\right)$$

After resolving the equation,

$$F_r = F_{xy}\cdot\cos(180^\circ - \arctan(F_x/F_y) - \varphi) \tag{7}$$

We knew that

$$\mu = \frac{F_t\cdot\sin(\alpha) + F_r\cdot\cos(\alpha)}{F_t\cdot\cos(\alpha) - F_r\cdot\sin(\alpha)}$$

Putting the value of the rake angle (α) of the tool inserts i.e. = 0

$$\mu = \frac{F_r}{F_t}$$

$$\mu = \frac{\cos(180^\circ - \arctan(F_x/F_y) - \varphi)}{\sin\left(180^\circ - \arctan\left(F_x/F_y\right) - \varphi\right)} \tag{8}$$

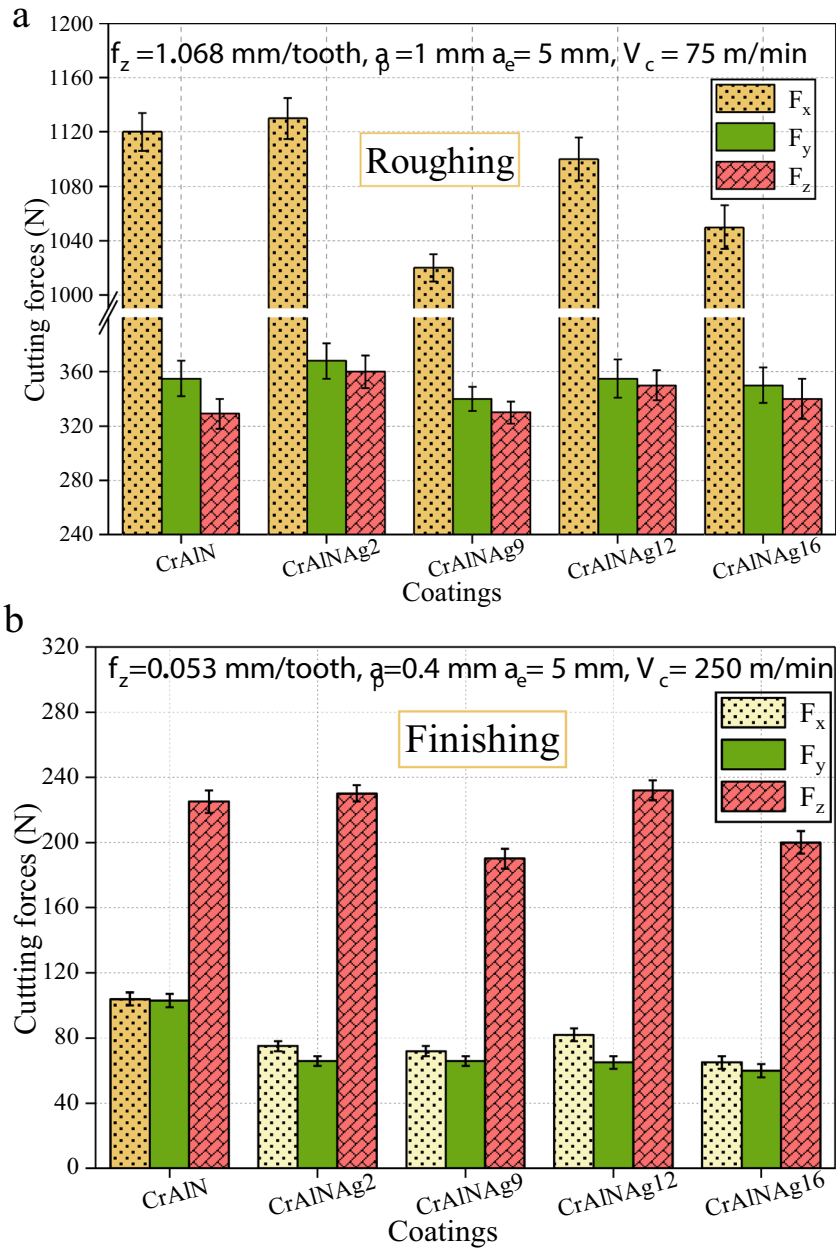

Fig. 10 Mean values of cutting forces during face milling with reference CrAlN and CrAlNAg-coated inserts under **a** roughing and **b** finishing operations

As discussed earlier, the angle of engagement plays a major role in cutting force (F_t) and feed force (F_r). Therefore, the forces under roughing conditions, calculated using Eqs. 3, 6, and 7, were plotted against the cutter engagement angle (ϕ) with the workpiece, as shown in Fig. 11. It is evident from the figure that F_x closely follows the trend of cutting force (F_t) [40, 41]. The variation in the feed force was explained by the cosine function as per the equations mentioned above. It is noteworthy that CrAlNAg9 coating was effective in bringing down cutting force and feed force compared to reference CrAlN coating and the other CrAlNAg coatings.

In order to gain further insight into the frictional behavior at the chip-tool interface during machining with coated tool inserts, the coefficient of friction was calculated using the formula indicated in Eq. 8. It is interesting to note that the trend of coefficient of friction (μ) for different coatings presented in Fig. 12 was matched with the coefficient of friction value which was obtained from the test in a ball-on-disc tribometer at a temperature of 600 °C in the previous work [32].

3.2.2 Chip temperature

Figure 13 presents a representative image depicting the chip's temperature profile formed during roughing conditions in milling, alongside the fluctuation of maximum

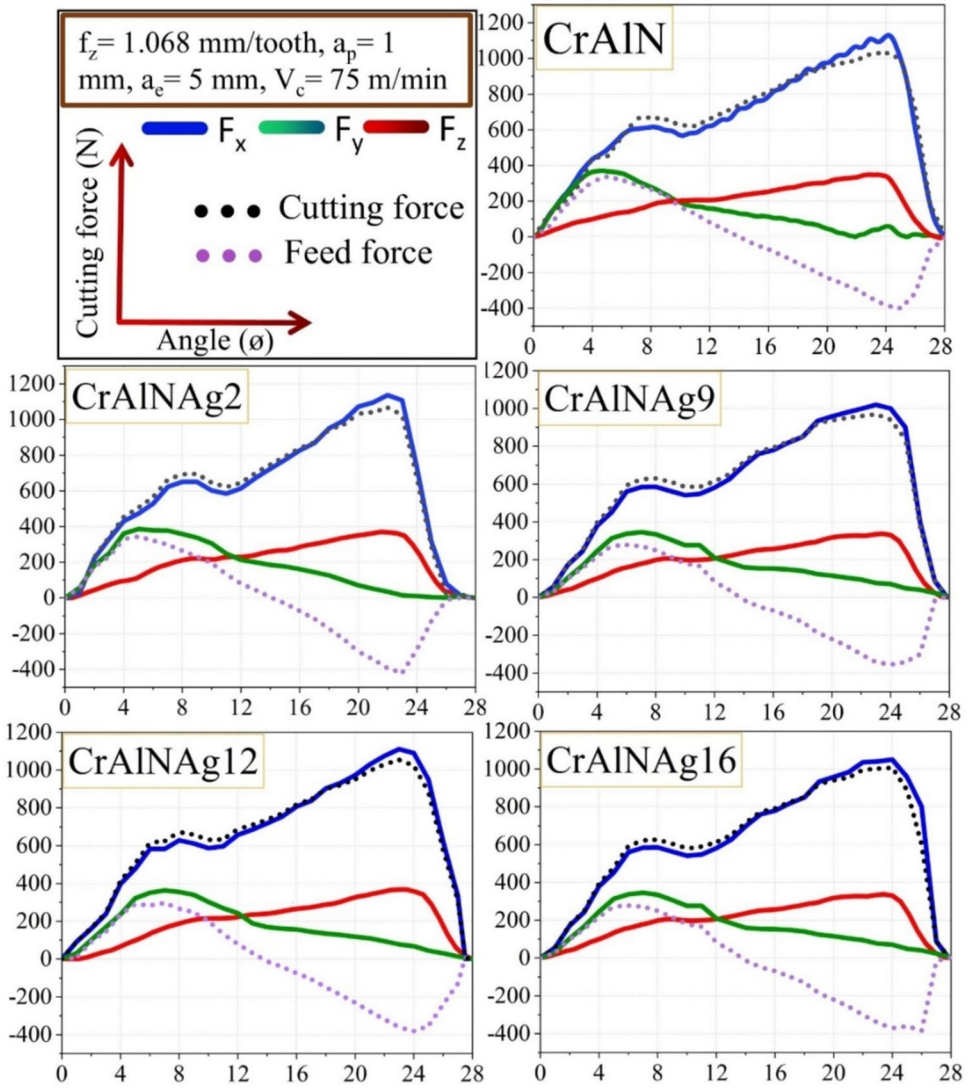

Fig. 11 Variation of different forces in face milling with the angle of engagement with the workpiece under roughing condition while using different coated tools

temperature over time while machining with CrAlNAg9-coated tool. The fluctuation pattern of the maximum temperature observed is the characteristic of milling operations, which involve intermittent cutting processes. A comparable intermittent nature of the force-related signals has been captured in Fig. 9.

Maximum chip temperatures for different coated tool inserts in face milling operation under a dry environment are presented in Fig. 14. It is obvious that rough milling produced lower chip temperature than finishing during machining. This is due to the lower cutting speed (75 m/min) associated with roughing than that of the finishing operation (with a cutting speed of 250 m/min). The addition of Ag in the coating, up to 2.4 at.%, did not result in a significant reduction in chip temperature. This is because such a low concentration does not provide a substantial lubricative effect during machining, leading to minimal improvement. However, increasing the Ag content to 8.6 at.% in CrAlN was found to be effective in reducing chip temperature by providing continuous lubrication throughout the machining process. The heat generated during machining drives the outward diffusion of the soft lubricant (Ag), enabling in-situ lubrication, which reduced chip temperature by approximately 11% compared to the reference CrAlN coating. In contrast, adding excessive Ag (as in CrAlNAg16 coating) compromises the balance between the soft phase (Ag) and the hard nitride phase of the coating. This leads to excessive outward diffusion and evaporation of Ag, causing a deficiency in lubrication over time. As a result, no further reduction in chip temperature was observed, with the reduction being limited to around 9%. It may be noted that there was no significant difference in chip temperature recorded during subsequent face milling operations, likely due to the absence of substantial tool wear under both roughing and finishing conditions. Therefore, these results were not presented here.

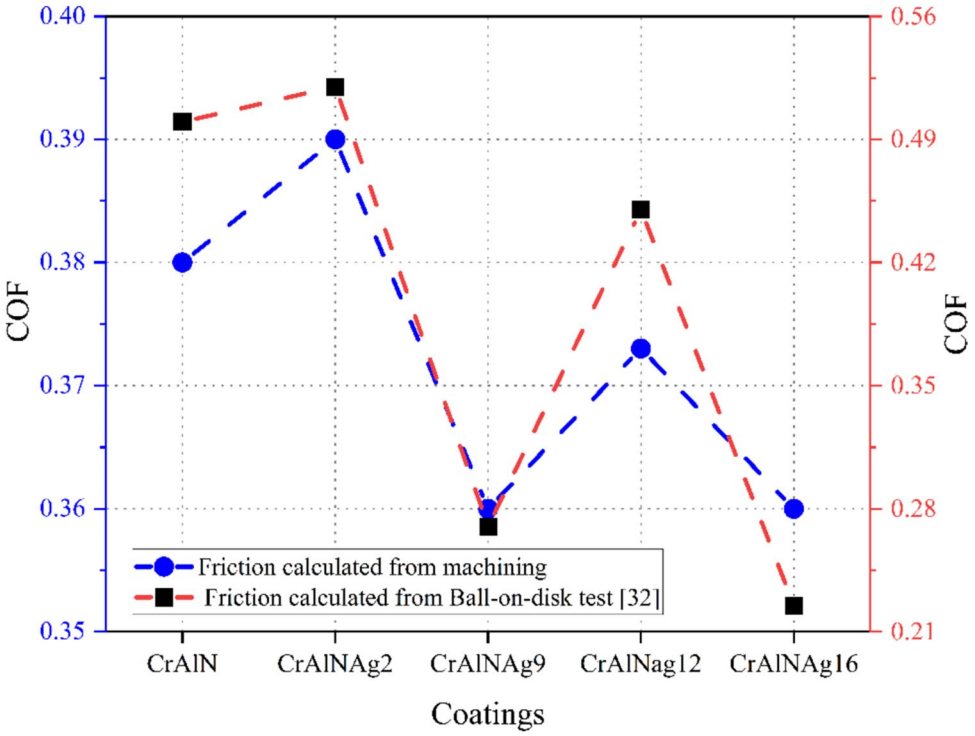

Fig. 12 Average coefficient of friction at the chip-tool interface during rough milling using different coated tools under a dry environment

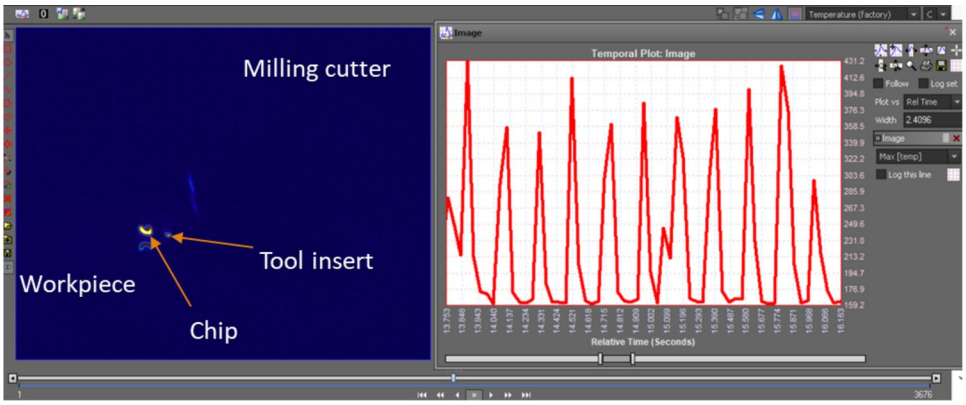

Fig. 13 Representative chip temperature profile while machining under roughing conditions using CrAlNAg9-coated tool (during 1st run)

3.2.3 Tool wear and surface roughness

Tool wear in roughing operation was primarily evaluated in terms of average flank wear using SEM and EDS, as shown in Fig. 15. While the average flank wear for reference CrAlN and CrAlNAg9-coated tools was comparable, the maximum flank wear was observed with the CrAlNAg16 coating, with the highest Ag content, followed by CrAlNAg12 coating. These results are in line with the those of specific wear rate previously reported by the authors [32]. EDS results presented in the same figure (Fig. 15) provided insight into the wear mechanisms during roughing-mode milling operations with CrAlN and CrAlNAg-coated tools.

The reference CrAlN coating showed significant adhesion of the work material as indicated in Fig. 15a1. Addition of Ag up to 8.6 at.% (CrAlNAg9 coating) was beneficial in mitigating the material sticking phenomenon while coating delamination was noticed for the coating with the highest Ag content (CrAlNAg16) due to improper adhesion. Elemental mapping of the CrAlNAg12-coated tool also revealed coating removal and adhesion of the work material. The location where the Cr signal was absent (probably signifying removal of coating), clearly showed the presence of Fe and O, suggesting the possible formation of FeO/Fe_2O_3 during machining. Formation of built-up layer (BUL) is, in particular, a more common occurrence in low-speed machining like in roughing operation. Therefore, it can be concluded that the addition of Ag up to 8.6 at.% was effective in restricting material adhesion during machining while ensuring the retention of the coating.

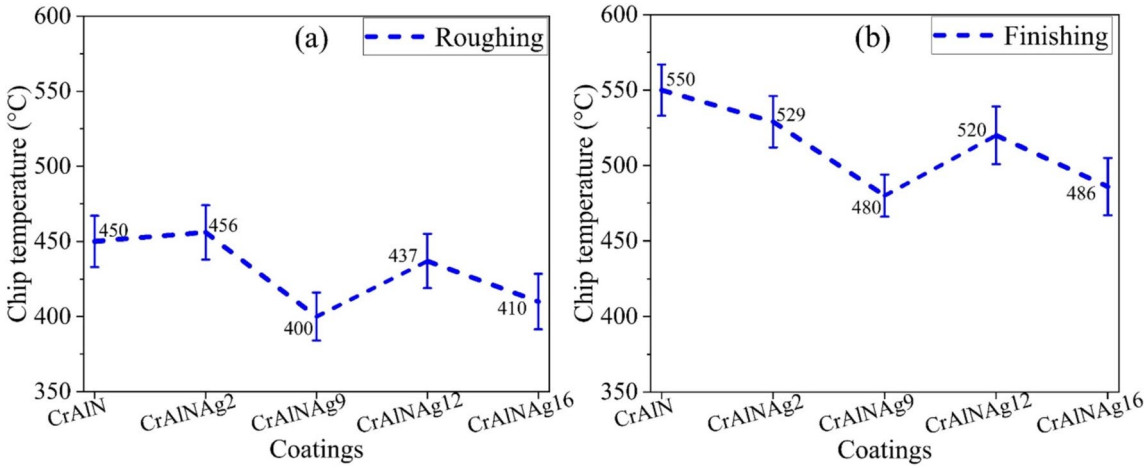

Fig. 14 Plot of maximum chip temperature generated during face milling with different coated tools under roughing and finishing operations (during 1st run)

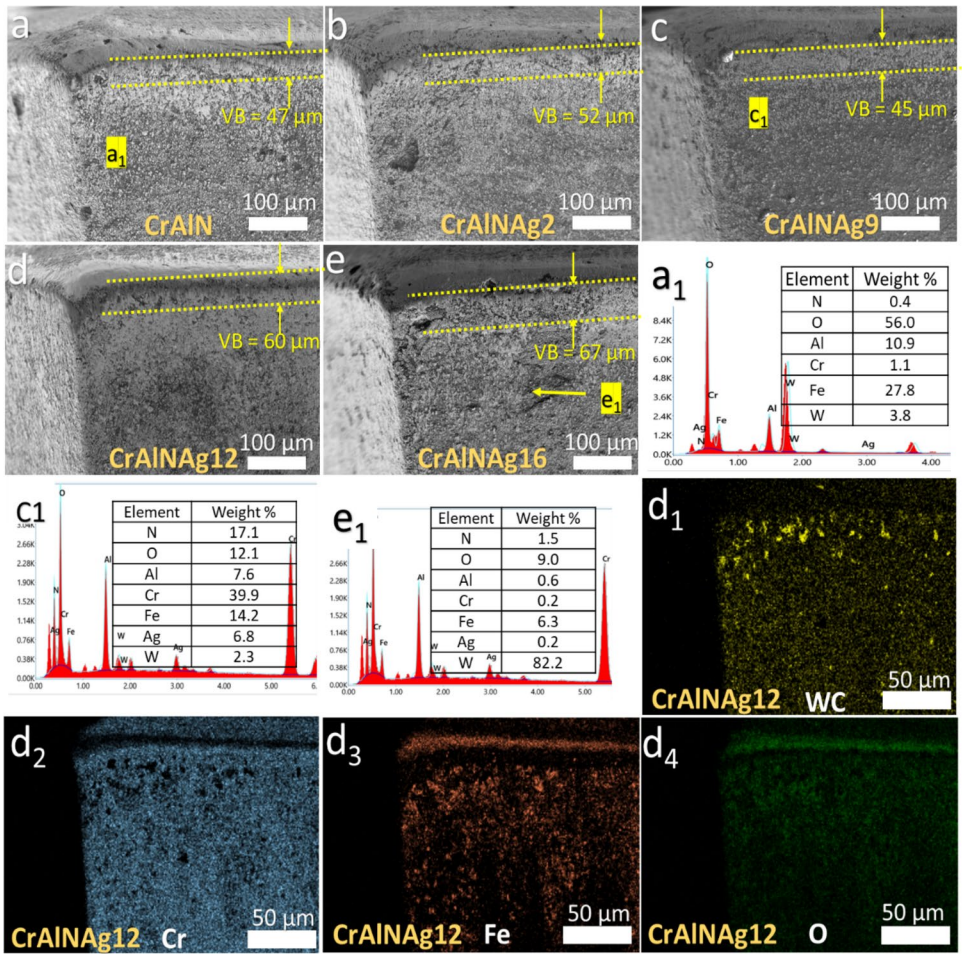

Fig. 15 SEM images of the flank surface of different coated tools along with the results of point EDS and elemental mapping under roughing operation after the 6th pass (720 mm length of cut)

Average flank wear under finishing mode was found to be slightly higher, as evident from the SEM images shown in Fig. 16. This increase was due to the higher cutting speed involved in the finishing operation and consequently higher cutting temperature. However, the trend of variation of average flank wear was similar, with the minimum flank wear

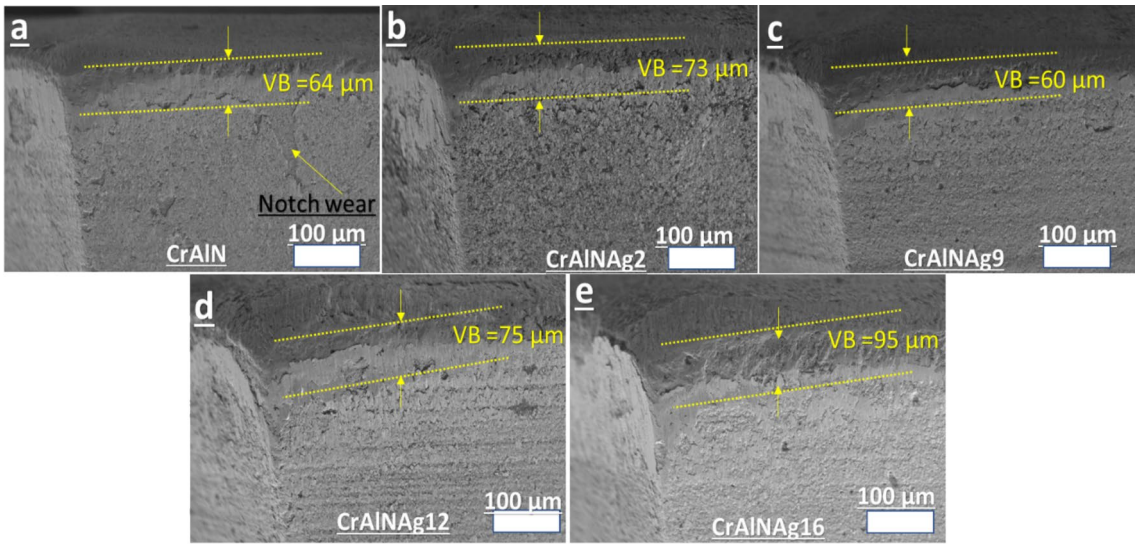

Fig. 16 SEM images of the flank surface of different coated tools under finishing operation after the 6th pass (720 mm length of cut)

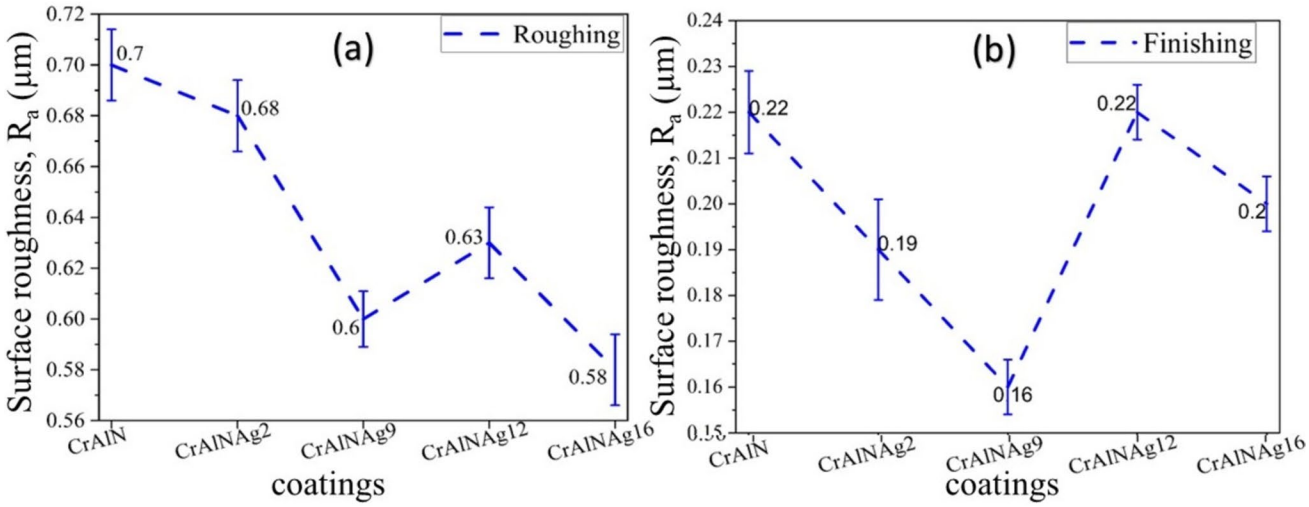

Fig. 17 Surface roughness of the machined workpiece (AISI 1045 steel) after face milling with reference CrAlN and CrAlNAg-coated tools under **a** roughing and **b** finishing conditions

achieved with the CrAlNAg9-coated tools and the worst flank wear recorded for CrAlNAg16-coated tools. Additionally, the CrAlN-coated tool demonstrated notch wear, as indicated in Fig. 16a.

The beneficial effect of Ag doping in the CrAlN coating was also evident in the results of the machined surface roughness, as shown in Fig. 17. Owing to superior low friction and anti-sticking properties of the CrAlNAg9 coating, material adhesion was restricted (as depicted in Fig. 15). This restriction resulted in a reduction in surface roughness by around 14% compared to that obtained with the reference CrAlN coated tool. At low cutting speed (i.e., under roughing condition), the CrAlNAg16 coating also demonstrated the benefits of low friction, resulting in reduced cutting forces, coefficient of friction, and cutting temperature, as shown in Figs. 10b, 12, and 14, respectively. Consequently, the CrAlNAg16 coating exhibited minimum surface roughness, signifying a reduction of around 17% compared to the reference CrAlN-coated tool. However, under finishing conditions, the CrAlNAg16 coating was not as effective as CrAlNAg9 in reducing surface roughness due to its inferior performance at high cutting speed. The CrAlNAg9 coating, owing to its greater wear resistance properties compared to other Ag-doped coatings, demonstrated the minimum surface roughness (~ 18% improvement compared to reference coating) under finishing condition as well. It is worth mentioning that, due to the

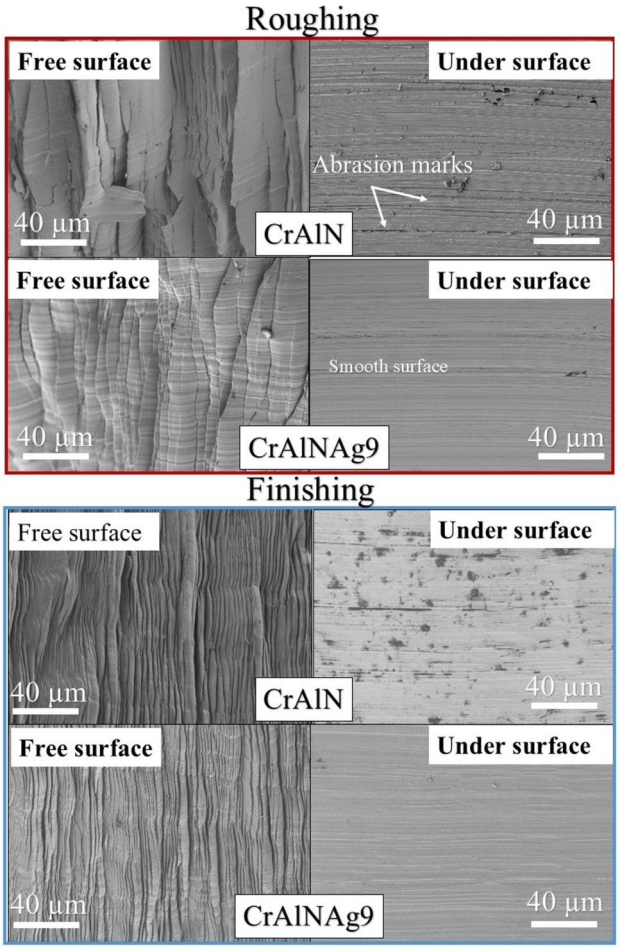

Fig. 18 Chip morphology on the free and back surfaces of the chips under roughing and finishing operations using CrAlNAg-coated milling inserts

tool's wiper edge feature, all the coated inserts deliver an improved overall surface finish.

3.2.4 Chip analysis

SEM images of the free and undersurface of generated chips during roughing and finishing modes of machining are depicted in Fig. 18. A laminar structure is visible on the free surface of the chips in both machining modes. However, the laminar structure was finer for chips generated during the finishing mode. It was also observed that this structure became finer while machining with the coated inserts under both the conditions. This laminar folding of the chip indirectly represents the shearing condition during machining. Therefore, it can be concluded that the finer structure resulted from improved shearing due to the lubrication provided by the Ag during the machining process. Notably, parallel stripes were visible on the undersurface, which could be attributed to irregular cutting edges and/or the presence of hard particles. However, the overall surface remained smooth.

The effect of Ag doping in CrAlN coating in roughing conditions was further studied by examining chip characteristics. Optical microscope images revealing a cross-section of the chip obtained with different coated tools are shown in Fig. 19. The effect of Ag as a solid lubricant is evident, as the CrAlNAg16 coating resulted in the minimum equivalent chip thickness (h_{ch}) due to reduced friction at the chip-tool interface under roughing conditions. The next lowest value of h_{ch} was achieved with CrAlNAg9 coating. Therefore, the results of cutting force, chip temperature, and surface roughness are in coherence with those of equivalent chip thickness.

Furthermore, previous researchers [32, 47–49] demonstrated that the use of anti-friction coatings was effective in reducing saw-tooth distance (P_c) and increasing chip serration frequency. The inclusion of Ag as a solid lubricant, particularly in CrAlNAg9 and CrAlNAg16 coating due to their low friction behavior, was found beneficial. The same effect was also visualized in the results of saw-tooth distance and chip serration frequency obtained with CrAlNAg-coated tools with different Ag content. The CrAlNAg16-coated tool exhibited the lowest saw-tooth distance and hence, the maximum serration frequency, owing to its low friction behavior under roughing conditions. On the other hand, under finishing conditions, the chips were too small to accurately reveal their characteristics; hence, they were not presented in this work.

4 Conclusions

The present study investigated the effect of Ag doping on the face milling performance of CrAlN-coated inserts under both roughing and finishing modes of machining. The results indicated that optimizing the Ag content in CrAlN coatings promoted the competitive growth of particles, leading to the formation of a dense columnar structure with enhanced cauliflower morphology. This structure improved the coating's hardness and adhesion strength compared to the reference CrAlN coating. The distribution of cutting forces varied significantly due to different depths of cut and the contribution of the cutting edges. Notably, the apparent coefficient of friction (COF) recorded during rough milling closely matched the trend observed in previous high-temperature tribological tests for the same coatings. Among the coatings tested, the CrAlNAg9-coated milling insert demonstrated superior performance by reducing various components of cutting force (F_x, F_y, and F_z) during both roughing and finishing operations. Specifically, CrAlNAg9-coated tools achieved a reduction in F_x by 10% and F_z by 15.5%

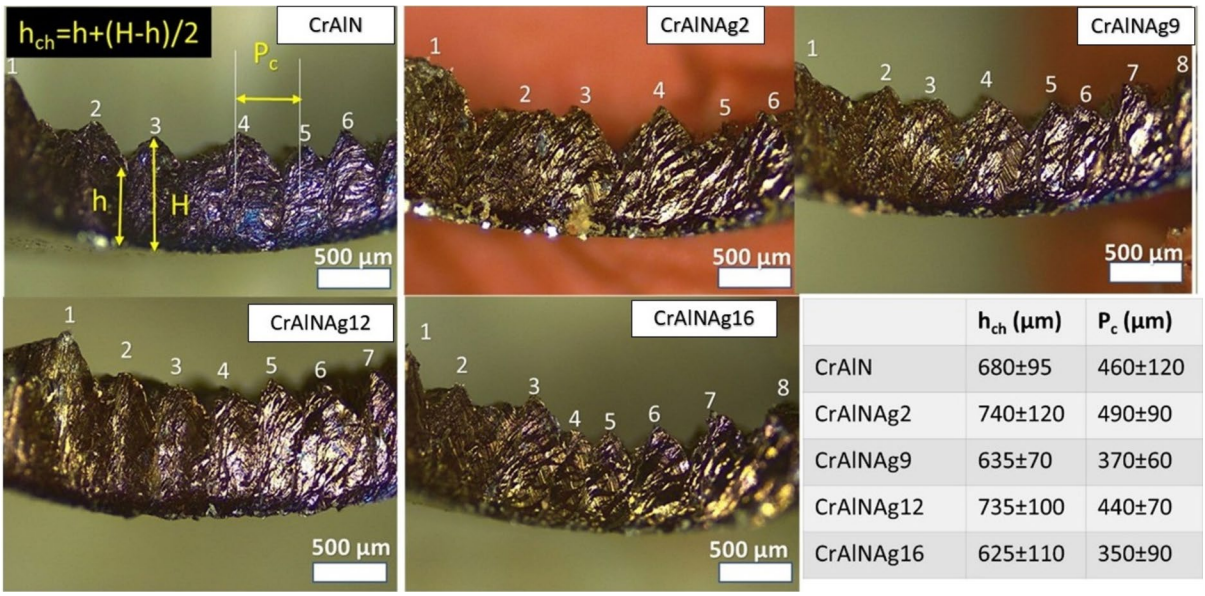

	h_{ch} (µm)	P_c (µm)
CrAlN	680±95	460±120
CrAlNAg2	740±120	490±90
CrAlNAg9	635±70	370±60
CrAlNAg12	735±100	440±70
CrAlNAg16	625±110	350±90

Fig. 19 Optical microscopic images of chips after face milling with reference CrAlN- and CrAlNAg-coated tools along with equivalent chip thickness (h_{Ch}), serration frequency, and saw-tooth distance (P_c)

during roughing and finishing operations, respectively, compared to the reference CrAlN-coated tools. Additionally, CrAlNAg9 and CrAlNAg16-coated inserts mitigated surface roughness by 14.2% and 17.2% during roughing and by 18.2% and 9.1% during finishing operations, respectively with reference to CrAlN-coated tools. These coatings also lowered chip temperature by over 11% and 9% compared to CrAlN-coated tools under both the milling conditions.

The results of this study are beneficial in selecting the optimal content of Ag as a soft phase in CrAlN nitride coatings to maximize performance in both roughing and finishing modes of milling of AISI 1045 steel.

Author contribution SSR: conceptualization, methodology, investigation, formal analysis, validation, writing—original draft, and writing—review and editing. CU: investigation, validation, writing, and editing. SG: supervision, conceptualization, investigation, validation, writing—review and editing, resources, project administration, and funding acquisition. FF: supervision, conceptualization, resources, project administration, and funding acquisition.

Funding The funding support received by Soumya Gangopadhyay from the Department of Science and Technology, Government of India in relation to an international collaborative project (no. DST/INT/Portugal/P-14/2017) between India and Portugal. Filipe Fernandes acknowledges the UIDB/00285/2020 and LA/P/0112/2020 projects, sponsored by FEDER Funds through Portugal 2020 (PT2020), the Competitiveness and Internationalization Operational Program (COMPETE 2020), and national funds through the Portuguese Foundation for Science and Technology (FCT). Support received through the bilateral collaborative project (no. 441.00 INDIA) between Portugal and India is also thankfully acknowledged.

Declarations

Ethics approval The authors claim that there are no ethical issues involved in this research.

Consent to participate All the authors consent to participate in this research and contribute to the research.

Consent for publication All the authors consent to publish the research. There are no potential copyright/plagiarism issues involved in this research.

Competing interests The authors declare no competing interests.

References

1. López de Lacalle LN, Lamikiz A, Salgado MA et al (2002) Process planning for reliable high-speed machining of moulds. Int J Prod Res 40:2789–2809. https://doi.org/10.1080/00207540210140068
2. Liu K, Li XP, Rahman M, Liu XD (2004) A study of the cutting modes in the grooving of tungsten carbide. Int J Adv Manuf Technol 24:321–326. https://doi.org/10.1007/s00170-003-1565-6
3. Arif M, Rahman M, San WY (2013) A study on the effect of tool-edge radius on critical machining characteristics in ultra-precision milling of tungsten carbide. Int J Adv Manuf Technol 67:1257–1265. https://doi.org/10.1007/s00170-012-4563-8
4. Cui X, Zhao J, Dong Y (2013) The effects of cutting parameters on tool life and wear mechanisms of CBN tool in high-speed face milling of hardened steel. Int J Adv Manuf Technol 66:955–964. https://doi.org/10.1007/s00170-012-4380-0
5. Cui X, Zhao J, Tian X (2013) Cutting forces, chip formation, and tool wear in high-speed face milling of AISI H13 steel with CBN tools. 1737–1749. https://doi.org/10.1007/s00170-012-4137-9
6. da Silva LR, da Silva OS, dos Santos FV et al (2019) Wear mechanisms of cutting tools in high-speed turning of Ti6Al4V alloy.

Int J Adv Manuf Technol 103:37–48. https://doi.org/10.1007/s00170-019-03519-2
7. Rajput SS, Upadhyay C, Gangopadhyay S, Fernandes F Effects of roughing, finishing, and aggressive machining conditions on the milling performance of AISI 1045 steel using TiAlN coated inserts. Proc Inst Mech Eng B J Eng Manuf 0:09544054231157963. https://doi.org/10.1177/09544054231157963
8. Mativenga PT, Hon KKB (2003) A study of cutting forces and surface finish in high-speed machining of AISI H13 tool steel using carbide tools with TiAlN based coatings. Proc Inst Mech Eng B J Eng Manuf 217:143–151. https://doi.org/10.1243/095440503321148786
9. Khrais SK, Lin YJ (2007) Wear mechanisms and tool performance of TiAlN PVD coated inserts during machining of AISI 4140 steel. Wear 262:64–69. https://doi.org/10.1016/j.wear.2006.03.052
10. Bouzakis KD, Gerardis S, Katirtzoglou G et al (2008) Increasing tool life by adjusting the milling cutting conditions according to PVD films' properties. CIRP Ann Manuf Technol 57:105–108. https://doi.org/10.1016/j.cirp.2008.03.070
11. Sreejith PS, Ngoi BKA (2000) Dry machining: machining of the future. J Mater Process Technol 101:287–291. https://doi.org/10.1016/S0924-0136(00)00445-3
12. Silva FJG, Martinho RP, Martins C et al (2019) Machining GX2CrNiMoN26-7-4 DSS alloy: wear analysis of TiAlN and TiCN/Al_2O_3/TiN coated carbide tools behavior in rough end milling operations. Coatings 9:392. https://doi.org/10.3390/COATINGS9060392
13. Fernández-Abia AI, Barreiro J, Fernández-Larrinoa J et al (2013) Behaviour of PVD coatings in the turning of austenitic stainless steels. Procedia Eng 63:133–141. https://doi.org/10.1016/j.proeng.2013.08.241
14. Upadhyay C, Rajput SS, Kumar CS, et al (2024) Performance evaluation of WC, SiAlON and SiCw + Al_2O_3 tools in dry machining of Inconel 617. J Manuf Process 109:235–249. https://doi.org/10.1016/j.jmapro.2023.12.006
15. Zheng G, Zhao G, Cheng X et al (2018) Frictional and wear performance of TiAlN/TiN coated tool against high-strength steel. Ceram Int 44:6878–6885. https://doi.org/10.1016/j.ceramint.2018.01.113
16. Arulkirubakaran D, Senthilkumar V (2017) Performance of TiN and TiAlN coated micro-grooved tools during machining of Ti-6Al-4V alloy. Int J Refract Metals Hard Mater 62:47–57. https://doi.org/10.1016/j.ijrmhm.2016.10.014
17. Upadhyay C, Rajput SS, Bera S, et al (2024) Influence of TiAlN coating thickness in dry machining of AISI 1045 steel using finite element simulation and experiments. Surf Coat Technol 131496. https://doi.org/10.1016/j.surfcoat.2024.131496
18. Rodríguez-Barrero S, Fernández-Larrinoa J, Azkona I et al (2016) Enhanced performance of nanostructured coatings for drilling by droplet elimination. Mater Manuf Processes 31:593–602. https://doi.org/10.1080/10426914.2014.973582
19. Kumar CS, Urbikain G, de Lacalle LNL, et al (2023) Investigating the effect of novel self-lubricant TiSiVN films on topography, diffusion and oxidation phenomenon at the chip-tool interface during dry machining of Ti-6Al-4V alloy. Tribol Int 186:. https://doi.org/10.1016/j.triboint.2023.108604
20. Kumar CS, Urbikain G, Fernandes F, et al (2024) Influence of V concentration in TiAlSiVN coating on self-lubrication, friction and tool wear during two-pass dry turning of austenitic steel 316 L. Tribol Int 193:. https://doi.org/10.1016/j.triboint.2024.109355
21. Kumar CS, Urbikain G, De Lucio PF et al (2024) Effect of V concentration in TiSiN monolayer coating on chip formation mechanism and chip sliding velocity during dry turning of Ti–6Al–4V alloy. J Market Res 32:4456–4464. https://doi.org/10.1016/j.jmrt.2024.09.007
22. Kumar CS, Urbikain G, De Lucio PF, et al (2023) Investigating the self-lubricating properties of novel TiSiVN coating during dry turning of Ti6Al4V alloy. Wear 532–533. https://doi.org/10.1016/j.wear.2023.205095
23. dos Santos GR, da Costa DD, Amorim FL, Torres RD (2007) Characterization of DLC thin film and evaluation of machining forces using coated inserts in turning of Al-Si alloys. Surf Coat Technol 202:1029–1033. https://doi.org/10.1016/j.surfcoat.2007.07.100
24. Rajput SS, Gangopadhyay S, Cavaleiro A et al (2021) Influence of Ag additions on the structure, mechanical properties and oxidation behaviour of CrAlNAg coatings deposited by sputtering. Surf Coat Technol 426:127767. https://doi.org/10.1016/j.surfcoat.2021.127767
25. Liu A, Deng J, Cui H, et al (2011) Oxidation resistance of CrN and CrAlN coating tools. In: Advanced Materials Research. pp 137–141 https://doi.org/10.4028/www.scientific.net/AMR.189-193.137.
26. Hu C, Xu YX, Chen L et al (2019) Mechanical properties, thermal stability and oxidation resistance of Ta-doped CrAlN coatings. Surf Coat Technol 368:25–32. https://doi.org/10.1016/j.surfcoat.2019.04.026
27. Pilkington A, Dowey SJ, Toton JT, Doyle ED (2013) Machining with AlCr-oxinitride PVD coated cutting tools. Tribol Int 65:303–313. https://doi.org/10.1016/j.triboint.2013.03.020
28. Fox-Rabinovich GS, Beake BD, Endrino JL et al (2006) Effect of mechanical properties measured at room and elevated temperatures on the wear resistance of cutting tools with TiAlN and AlCrN coatings. Surf Coat Technol 200:5738–5742. https://doi.org/10.1016/j.surfcoat.2005.08.132
29. Liu W, Chu Q, Zeng J et al (2017) PVD-CrAlN and TiAlN coated Si3N4 ceramic cutting inserts-2. High speed face milling performance and wear mechanism study. Ceram Int 43:9488–9492. https://doi.org/10.1016/j.ceramint.2017.04.127
30. Kumar KM, Mathew NT, Baburaj M (2021) Sustainable milling of Ti-6Al-4 V super alloy using AlCrN and TiAlN coated tools. Mater Today Proc 50:1732–1738. https://doi.org/10.1016/j.matpr.2021.09.175
31. Chen L, Liu ZQ, Xu YX, Du Y (2015) Influence of Zr on structure, mechanical and thermal properties of Cr-Al-N coatings. Surf Coat Technol 275:289–295. https://doi.org/10.1016/j.surfcoat.2015.05.004
32. Rajput SS, Gangopadhyay S, Yaqub TB, et al (2022) Room and high temperature tribological performance of CrAlN(Ag) coatings: the influence of Ag additions. Surf Coat Technol 450. https://doi.org/10.1016/j.surfcoat.2022.129011
33. Fernandes F, Al-Rjoub A, Cavaleiro D et al (2020) Room and high temperature tribological performance of multilayered tisin/tin and tisin/tin(Ag) coatings deposited by sputtering. Coatings 10:1–13. https://doi.org/10.3390/coatings10121191
34. Rajput SS, Upadhyay C, Gangopadhyay S, Fernandes F (2024) High-temperature tribological behaviour and machining performance of self-lubricant CrAlNAg coatings for dry milling operations. Tribol Int 109824. https://doi.org/10.1016/j.triboint.2024.109824
35. Rajput SS, Bhangale A, Moharana A, et al (2023) Effect of Ag addition on the oxidation behavior of CrAlN coating at elevated temperatures. Mater Today Proc. https://doi.org/10.1016/j.matpr.2023.06.337
36. Basnyat P, Luster B, Kertzman Z et al (2007) Mechanical and tribological properties of CrAlN-Ag self-lubricating films. Surf Coat Technol 202:1011–1016. https://doi.org/10.1016/j.surfcoat.2007.05.088
37. Cavaleiro D, Veeregowda D, Cavaleiro A et al (2020) High temperature tribological behaviour of TiSiN(Ag) films deposited by

HiPIMS in DOMS mode. Surf Coat Technol 399:126176. https://doi.org/10.1016/j.surfcoat.2020.126176
38. Aouadi SM, Singh DP, Stone DS et al (2010) Adaptive VN/Ag nanocomposite coatings with lubricious behavior from 25 to 1000 °c. Acta Mater 58:5326–5331. https://doi.org/10.1016/j.actamat.2010.06.006
39. Fernández Landeta J, Fernández Valdivielso A, de Lacalle LN et al (2015) Wear of form taps in threading of steel cold forged parts. J Manuf Sci Eng 137:31002. https://doi.org/10.1115/1.4029652
40. Kundrák J Theoretical and experimental analysis of the effect of chip size ratio on cutting forces in face milling of steel. 3:29–35
41. Kundrák J, Markopoulos AP, Makkai T, et al (2018) Analysis of the effect of feed on chip size ratio and cutting forces in face milling for various cutting speeds. Manufacturing Technology 18:431–438. https://doi.org/10.21062/ujep/117.2018/a/1213-2489/MT/18/3/431
42. Hosseini E, Rehman S, Alimoradi A (2021) Optimization of turn-milling process in roughing and finishing regimes: trade-off between productivity, cutting force and surface integrity. Proceedings of the Institution of Mechanical Engineers, Part E: Journal of Process Mechanical Engineering 235:1383–1395. https://doi.org/10.1177/0954408921998513
43. Cui X, Guo J, Zhao J, Yan Y (2015) Chip temperature and its effects on chip morphology, cutting forces, and surface roughness in high-speed face milling of hardened steel. Int J Adv Manuf Technol 77:2209–2219. https://doi.org/10.1007/s00170-014-6635-4
44. Li HZ, Zeng H, Chen XQ (2006) An experimental study of tool wear and cutting force variation in the end milling of Inconel 718 with coated carbide inserts. J Mater Process Technol 180:296–304. https://doi.org/10.1016/j.jmatprotec.2006.07.009
45. Vergne C, Boher C, Levaillant C, Gras R (2001) Analysis of the friction and wear behavior of hot work tool scale: application to the hot rolling process. Wear 250–251:322–333. https://doi.org/10.1016/S0043-1648(01)00598-1
46. Dohda K, Boher C, Rezai-Aria F, Mahayotsanun N (2015) Tribology in metal forming at elevated temperatures. Friction 3:1–27. https://doi.org/10.1007/s40544-015-0077-3
47. Al-Rjoub A, Cavaleiro A, Rajput SS, Fernandes F (2021) High Si multilayered TiSiN/TiN(Ag) films with superior oxidation resistance. J Market Res 12:2340–2347. https://doi.org/10.1016/j.jmrt.2021.04.040
48. Li J, Li P, Guo H, Zhang Z (2017) Study on the formation mechanism of saw-tooth chip in high-speed cutting process. Proc Inst Mech Eng B J Eng Manuf 231:2577–2584. https://doi.org/10.1177/0954405416634277
49. Thakur A, Gangopadhyay S (2018) Evaluation of micro-features of chips of Inconel 825 during dry turning with uncoated and chemical vapour deposition multilayer coated tools. Proc Inst Mech Eng B J Eng Manuf 232:979–994. https://doi.org/10.1177/0954405416661584